JOURNAL OF AIRCRAFT
Vol. 44, No. 1, January–February 2007

Engineering Notes

ENGINEERING NOTES are short manuscripts describing new developments or important results of a preliminary nature. These Notes should not exceed 2500 words (where a figure or table counts as 200 words). Following informal review by the Editors, they may be published within a few months of the date of receipt. Style requirements are the same as for regular contributions (see inside back cover).

Effect of Flap Motion on Unsteady Aerodynamic Loads

T. Lee* and P. Gerontakos†
McGill University, Montreal, Quebec H3A 2T5, Canada

DOI: 10.2514/1.25172

I. Introduction

THE dynamic overshoots in helicopter rotor blade lift force and the torsional and control loads, as a result of large cyclic pitch variations imposed on the rotor blades to avoid aircraft roll in forward flight, continue to make dynamic stall and its control an important topic in rotorcraft engineering. Additionally, a large amount of hysteresis is also present in all three lift, drag, and pitching moments of the airloads. The hysteresis effects, associated with the dynamic-stall phenomena, were the source of reduced aerodynamic damping, which can potentially lead to a variety of aeroelastic problems on the rotor blades. Various passive and active dynamic-stall flow control concepts, such as the use of trailing-edge flaps (TEFs), pulsating and synthetic jets, leading-edge blowing and suction, dynamically deformable leading edges, etc., capable of alleviating the detrimental hysteresis in the nonlinear airloads, as well as ensuring positive aerodynamic damping, have been attempted. Among them, the active control via a dynamically deflecting trailing-edge flap [1–5], integrated with the main lifting section of the blade and deflected cyclically to control the lift and/or moment characteristics of the blade section, has been used extensively by researchers elsewhere. Feszty et al. [4] studied computationally the reduction of the large negative pitching moment on a NACA 0012 wing, oscillated with $\alpha(t) = 15\,\text{deg} + 10\,\text{deg}\,\sin\omega t$ at a reduced frequency $\kappa\,(\pi f_o c/u_o$, where f_o is the wing oscillation frequency, c is the chord, and u_o is the freestream velocity) of 0.173, via a pulsed trailing-edge flap. Their computational fluid dynamics (CFD) results show that optimum pulsed TEF motions, represented by $\delta(t) = \delta_{\max}[1-\cos(t/t_d)]$, with an upward flap deflection of $\delta_{\max} = 20\,\text{deg}$, a flap duration t_d of about one-third of the airfoil motion time period, and a start time in the third quarter of the azimuth are required to provide a reduction in the negative pitching-moment coefficient C_m. Gerontakos and Lee [5] measured the detailed surface pressure distributions of an oscillating NACA 0015 wing, equipped with a moveable 25%-chord TEF. Similar to the pulsed flap motion employed by Feszty et al., the flap actuation consisted of a brief pulse, represented by a constant ramp-up motion, remained steady briefly, and was followed by a constant ramp-down motion. The main wing was undergoing a deep-stall oscillation with $\alpha(t) = 15\,\text{deg} + 10\,\text{deg}\,\sin\omega t$ and $\kappa = 0.1$, and was superimposed with prescheduled TEF motions with $\delta_{\max} = \pm 7.5$ and $\pm 15\,\text{deg}$; $t_s = -0.5\pi$, 0π, and 0.5π (corresponding to a flap actuation at the minimum angle of attack $\alpha_{\min}$, mean α_m, and maximum $\alpha_{\max}$, respectively); and $t_d = 0.35\,f_o^{-1}$ to $0.5\,f_o^{-1}$. They further concluded that a relatively early flap actuation [initiated between α_m (less than α_{ss}) and $\alpha_{\max}$ during pitch-up; that is, during the later part of the second quarter of the azimuth] and a rather long duration (about 50% of the oscillation cycle time f_o^{-1}), in conjunction with an upward flap deflection (with $\delta_{\max} > \Delta\alpha$), should be more effective in reducing the nose-down pitching-moment excursion and in providing a good compromise between negative damping and maximizing dynamic lift. Also, the leading-edge vortex (LEV) formation and detachment were not affected by the TEF motion, although the low pressure signature or footprint of the LEV was, however, reduced by the upward flap deflection. More important, the reduction in $|-C_{m,\text{peak}}|$ was found to be mainly a consequence of the suction pressure introduced on the lower surface of the control flap. The effects of the TEF control of the dynamic-load loops of a wing subjected to attached-flow and light-stall oscillations [5], however, were not reported.

The objective of this study was to investigate the effects of TEF motion on the unsteady aerodynamic loads of a NACA 0015 wing oscillated through the static-stall angle α_{ss} (an extension of the work of Gerontakos and Lee [5]). Special emphasis was given to the characterization of the effects of t_s and $\delta_{\max}$ (at fixed $t_d = 0.5\,f_o^{-1}$) of the flap motion on the behavior of the phase-locked ensemble-averaged dynamic $C_l - C_m$ load loops, obtained from the integration of surface pressure distributions, over one oscillation cycle. Cross-hot-wire wake flow measurements were also made to supplement the surface pressure measurements.

II. Experimental Methods

The experiment was conducted in a $0.9 \times 1.2 \times 2.7$ m suction-type wind tunnel with a freestream turbulence intensity of 0.03% at $u_o = 15$ m/s at McGill University. A rectangular NACA 0015 wing, equipped with a 25% c full-span trailing-edge flap of a simple-hinged type, with $c = 25.4$ cm and a semispan of 38 cm, was used as the test model. The main wing was oscillated by a specially designed four-bar linkage mechanism, capable of oscillating the airfoil sinusoidally at various α_m, $\Delta\alpha$, and f_o. The airfoil pitch axis was located at the one-quarter chord location, and f_o was measured to an accuracy of ± 0.02 Hz through a potentiometer mounted on the servomotor shaft. The wing was oscillated through $\alpha_{ss}(16.5\,\text{deg})$ with $\Delta\alpha = 6\,\text{deg}$ and $\alpha_m = 12$ and 14 deg (corresponding to attached-flow and light-stall oscillation, respectively) at $\kappa = 0.1$ and $Re = 1.65 \times 10^5$. The TEF was activated and deactivated independently by a Futaba model S-3003 servomotor located at the wing root and driven by a custom-built controller, which actuated the flap in response to the wing phase signal $\tau = \omega t$. The TEF actuation employed a brief pulse, represented by a constant ramp-up motion, remained steady briefly, and was followed by a constant ramp-down motion, which was actuated at any τ and α. The ramp-up and ramp-down times were each approximately 8% of the time required for the wing to undergo one full cycle of oscillation. Both upward and downward flap deflections ($\delta_{\max} = \pm 7.5\,\text{deg}$) at selected t_s (-0.5π, 0π, and 0.5π) and t_d ($0.5\,f_o^{-1}$) were tested. Table 1 lists the parameters that describe the flap actuation profile in various units. The surface pressure distributions were obtained from 48 0.35-mm-diam pressure taps,

Received 16 May 2006; revision received 12 October 2006; accepted for publication 16 October 2006.

*Associate Professor, Department of Mechanical Engineering.
†Graduate Research Assistant, Department of Mechanical Engineering.

Table 1 TEF parameters and critical aerodynamic values

Case	$\delta_{\max}$	t_s	t_s[a]	t_{ss}[b]/t_e[c]	t_e[a,c]	$C_{l,\max}$	α_{ds}	$C_{d,\max}$	$C_{m,\text{peak}}$	$C_{w,\text{ccw}}$	$C_{w,\text{cw}}$	$C_{w,\text{net}}$[d]
$\alpha(t) = 12\deg + 6\deg \sin\omega t$												
Baseline wing						1.09	-	0.13	-	0.32	0.00	0.32
1	+7.5 deg	-0.5π	6 $\deg_u$	0.40	18 $\deg_d$	1.09	-	0.13	-	0.00	−0.43	−0.43
2	+7.5 deg	0π	12 $\deg_u$	0.39	12 $\deg_d$	0.89	-	0.09	-	0.28	0.00	0.28
3	+7.5 deg	0.5π	18 $\deg_u$	0.40	6 $\deg_u$	1.11	-	0.13	-	1.03	0.00	1.03
4	−7.5 deg	-0.5π	6 $\deg_u$	0.40	18 $\deg_d$	1.27	-	0.16	-	0.87	0.00	0.87
5	−7.5 deg	0π	12 $\deg_u$	0.35	12 $\deg_d$	1.34	18.0	0.41	−0.167	0.18	−0.34	−0.16
6	−7.5 deg	0.5π	18 $\deg_u$	0.36	6 $\deg_u$	1.21	17.7	0.37	−0.148	0.06	−0.94	−0.88
$\alpha(t) = 14\deg + 6\deg \sin\omega t$												
Baseline wing						1.23	19.9	0.40	−0.119	0.11	−0.42	−0.31
7	+7.5 deg	-0.5π	8 $\deg_u$	0.38	20 $\deg_d$	1.18	20.0	0.40	−0.117	0.04	−1.07	−1.03
8	+7.5 deg	0π	14 $\deg_u$	0.37	14 $\deg_d$	1.07	19.9	0.33	−0.057	0.10	−0.48	−0.38
9	+7.5 deg	0.5π	20 $\deg_u$	0.36	8 $\deg_u$	1.22	19.8	0.41	−0.123	0.35	−0.14	0.21
10	−7.5 deg	-0.5π	8 $\deg_u$	0.35	20 $\deg_d$	1.35	19.7	0.42	−0.130	0.35	−0.09	0.26
11	−7.5 deg	0π	14 $\deg_u$	0.36	14 $\deg_d$	1.44	19.8	0.52	−0.213	0.12	−0.19	−0.07
12	−7.5 deg	0.5π	20 $\deg_u$	0.36	8 $\deg_u$	1.25	20.0	0.45	−0.181	0.04	−0.89	−0.85

[a]Subscripts u and d denote pitch-up and pitch-down, respectively.
[b]Steady-state time period.
[c]End of flap actuation.
[d]Net torsional damping factor.

covering up to $x/c = 0$ to 96.3%, distributed over the upper and lower surfaces of the wing model. The pressure signals were phase-locked ensemble-averaged over 100 cycles of oscillation and were integrated numerically to compute the unsteady aerodynamic loads and pitching moments. An uncertainty analysis gives a typical total uncertainty ± 0.013 in C_p. The wake velocity profiles were also examined by using a miniature cross-hot-wire probe at $x/c = 1.0$. Details of the experimental setup and methods are given in Gerontakos and Lee [5].

III. Results and Discussion

The attached-flow and light-stall oscillations were established first from the drastic change in the characteristics of the hysteresis loop, particularly the $C_m - \alpha$ loop, as α_m was increased from 12 to 14 deg (Fig. 1). The light-stall oscillation (with $\alpha_m = 14$ deg) introduced a second clockwise (CW) C_m loop of negative damping, in addition to the single C_m loop associated with attached-flow oscillation (with $\alpha_m \leq 12$ deg) and gave rise to figure-eight-like behavior. The peak pitching-moment coefficient $-C_{m,\text{peak}}$ and the dynamic-stall angle α_{ds} were found to occur at $\alpha_{\max}$ or at the end of the pitch-up motion, as a result of the "premature spillage" of the LEV. For a baseline, or uncontrolled, NACA 0015 wing oscillated slightly through α_{ss} with $\alpha_m = 12\deg$, the dynamic $C_l - \alpha$ loop, however, exhibited an attached-flow-like oscillation; that is, no significant hysteresis was noticed nor was there a significant increase in the $C_{l,\max}$. Note that for deep-stall oscillation (i.e., $\alpha(t) = 16\deg + 6\deg \sin\omega t$), a third loop in the counterclockwise (CCW) sense (a characteristic of deep-stall oscillations [6]) was observed, suggesting that more positive, or CCW, torsional damping was restored when deep-stall penetration occurred and was with $-C_{m,\text{peak}}$, occurring before α_{ds}. The torsional damping factor C_w was defined by the line integral [5,7]

$$C_w = \int C_m(\alpha)\mathrm{d}\alpha = \int_{\text{ccw}} C_m(\alpha)\mathrm{d}\alpha + \int_{\text{cw}} C_m(\alpha)\mathrm{d}\alpha$$

Note that C_w is positive when it corresponds to a CCW loop and negative for a CW loop in the C_m vs α curve.

The effect of upward TEF motions actuated at selected t_s on C_l and C_m for a NACA 0015 wing oscillated slightly through α_{ss} with $\alpha(t) = 12\deg + 6\deg \sin\omega t$ was examined first (Fig. 2). The critical aerodynamic and C_w values are listed in Table 1. Similar to a static wing equipped with an upward flap, a reduction in C_l and negative damping of an oscillating NACA wing with an upward TEF actuated at α_m, or $t_s = 0\pi$ (case 2; Figs. 2a and 2d), during pitch-up, as a result of induced negative camber effects, especially in the trailing-edge region, was observed. For an upward flap actuated at $\alpha_{\max}$ during pitch-down (case 3), a 220% increase in the positive damping, or $C_{w,\text{ccw}}$, accompanied by a significantly decreased C_l during flap actuation, was observed. It is, however, interesting to note that for an upward flap actuated at $\alpha_{\min} = 6$ deg, or $t_s = -5\pi$, during pitch-up (case 1), the significantly reduced C_l also led to a single CW C_m–α loop (Fig. 2c) compared with a CCW C_m–α loop of a baseline wing (Fig. 1b); a $C_{w,\text{net}}$ of −0.43, compared with 0.32 of a baseline wing, was observed.

For a downward-deflected TEF, the behavior of the dynamic-load loops was somewhat unexpected; depending on the magnitude of t_s,

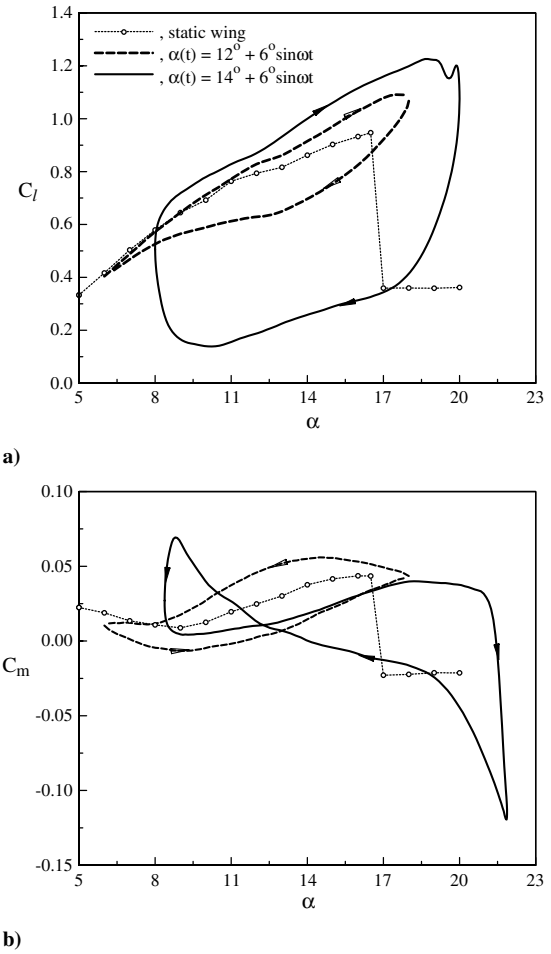

Fig. 1 Dynamic C_l and C_m loops.

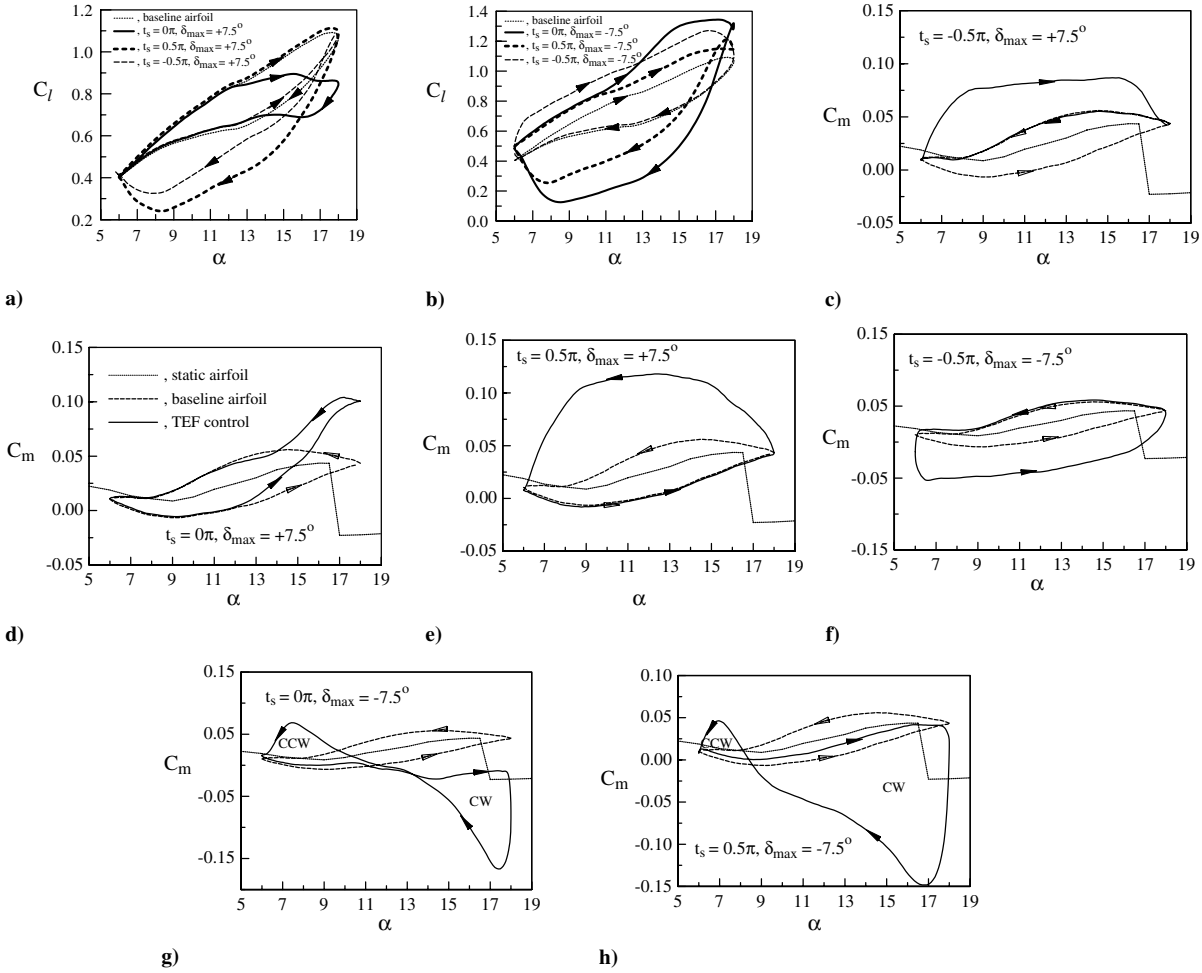

Fig. 2 TEF control of dynamic C_l and C_m loops for $\alpha(t) = 12\,\text{deg} + 6\,\text{deg}\,\sin\omega t$.

the dynamic C_l and C_m loops of an otherwise attached-flow oscillation (characterized by a single CCW C_m loop and a small C_l hysteresis) could exhibit a light-stall-like oscillation. For $t_s = -0.5\pi$, or a flap actuated at $\alpha_{\min}$ during pitch-up (case 4), the C_l–α curve was shifted vertically upward (Fig. 2b), due to the induced positive camber effects and the subsequent body-conforming flow improvement, especially in the trailing-edge region. The increase in the lift-curve slope also rendered a strengthened CCW C_m loop or $C_{w,\text{ccw}}$, compared with a baseline wing (Fig. 2f). For a TEF actuated at α_m and $\alpha_{\max}$ during pitch-up and pitch-down, respectively, (cases 5 and 6), there was a presence of a LEV-induced CW C_m loop (Figs. 2g and 2h), or a negative C_w value, compared with a baseline-wing oscillation. The strength of the LEV and the post-stall drop in C_l was found to be decreased with increasing t_s; that is, the earlier the flap actuation, the stronger the LEV and the larger the post-stall lift loss and C_l hysteresis, as a consequence of the TEF suppression of the viscous effects in the trailing-edge region, in addition to the induced positive camber effects and the virtual increase in the effective angle of attack, compared with a baseline wing. The body-conforming flow induced in the trailing-edge region also increased the effective $\alpha_{\max}$, thus allowing the initiation, convection, and shedding of a premature LEV. This unusual presence of a rather weak LEV and its subsequent detachment from the wing upper surface can also be demonstrated from the variation in the C_p distributions (Fig. 3) and the associated increase in the wake deficit and width and fluctuating velocities u' (Fig. 4).

Figure 3 shows the representative surface pressure coefficient C_p distributions at $\alpha_u = 18$ deg during pitch-up and $\alpha_d = 17$ and 8 deg during pitch-down, with and without TEF control. Also shown in Fig. 3 are the C_p distributions of a static NACA 0015 at the same α. For a NACA 0015 wing oscillated slightly through α_{ss} with $\alpha_{\max} = 18$ deg, the existence of an attached boundary-layer flow and the absence of a LEV and flow separation for an upward TEF actuated at α_m during pitch-up (Figs. 3a and 3b), similar to those observed for a baseline wing, can be clearly seen. Also, both the suction and positive pressures on the upper and lower wing surfaces were, however, decreased, especially on the upper and lower surfaces of the flap, compared with a baseline wing. Note the flat C_p distribution of a static wing for $\alpha \geq \alpha_{ss}$. Figure 3c further indicates that during the later portion of the pitch-down motion when the flap returned to its undeflected position, no noticeable discrepancy in the C_p values was observed relative to the baseline case, therefore implying that an upward flap motion does not affect the overall flow characteristics. The reappearance of a laminar separation bubble for $\alpha_d \leq 8$ deg is also evident. In contrast to an upward TEF, for a downward TEF, the formation of a weak LEV and its detachment from the wing upper surface and the resulting increase in C_l and $C_{l,\max}$ can be clearly identified from the C_p distributions shown in Figs. 3a and 3b. The observed decrease of the undesirable nose-down pitching moment was mainly due to the presence of suction pressure on the lower surface of the flap.

The influence of the TEF motion on C_l, C_m, and C_p can also be reflected from the modification of the wake flow structures presented in Fig. 4. The upward TEF motion was efficient in containing a reduced momentum deficit throughout the oscillation cycle, resulting in a reduced drag and a slightly narrowed wake width during pitch-up, which was accompanied by a slightly reduced streamwise velocity fluctuation u'. The shape of the wake profile, however, was not dramatically altered, compared with a baseline wing, though its centerline was shifted upwards. The upward flap deflection weakened the turbulent kinetic energy and, presumably, the Reynolds stress as well, and thus decreased the drag force (Table 1). Note also the pronounced reduction in the wake width for an

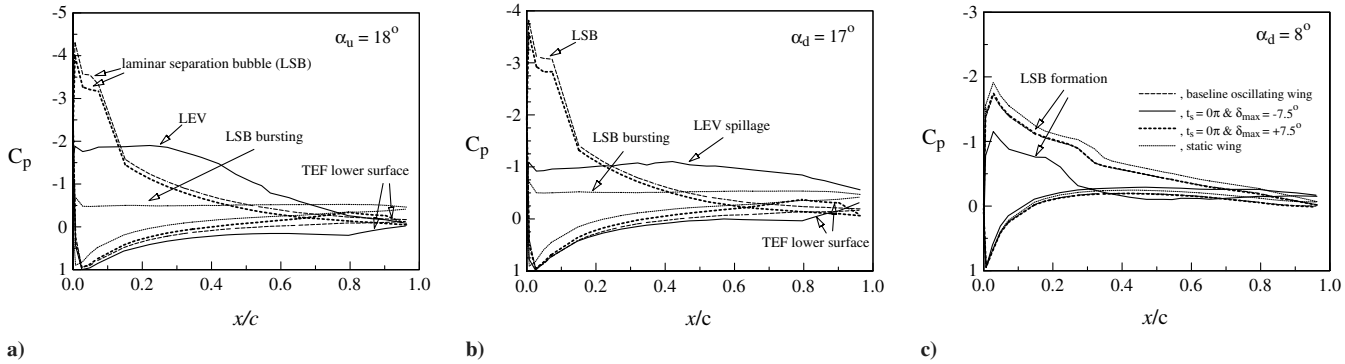

Fig. 3 C_p distributions for $\alpha(t) = 12\,\text{deg} + 6\,\text{deg}\,\sin\omega t$.

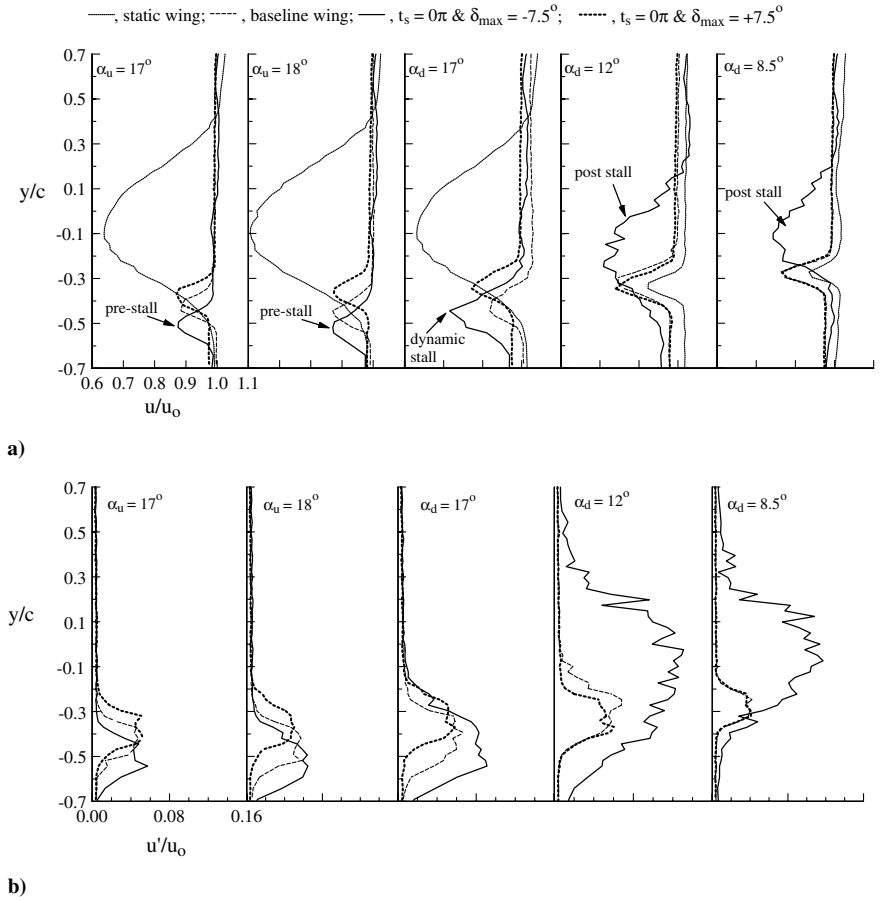

Fig. 4 Typical wake flow structures for $\alpha(t) = 12\,\text{deg} + 6\,\text{deg}\,\sin\omega t$.

oscillating wing, as a result of the boundary-layer improvement effects, compared with a static wing at the same α. A substantial increase in the wake width and deficit and wake velocity fluctuations was, however, observed for a downward flap actuated at $t_s = 0\pi$, or α_m, as a consequence of LEV formation and its premature spillage from the wing upper surface, compared with a baseline wing.

The TEF control of the dynamic C_l and C_m loops for a NACA 0015 wing undergoing a light-stall oscillation with $\alpha(t) = 14\,\text{deg} + 6\,\text{deg}\,\sin\omega t$ was also investigated and represented in Figs. 5a and 5b. The upward TEF deflection primarily provided a mitigation of the excessive nose-down C_m produced by the transient LEV effects (Fig. 5b). The phase angles at which the formation, convection, and detachment of the LEV was found to be virtually unaffected by the upward TEF motion. The low pressure signature or footprint of the premature LEV was, however, reduced, compared with a baseline wing (Fig. 5c). The LEV was not present until $\alpha_u \approx 19.2\,\text{deg}$, and the detachment occurred at $\alpha_{ds} = 19.8\,\text{deg}$ ($\approx\alpha_{\max} = 20\,\text{deg}$) for a baseline wing. The downward TEF motion-induced positive effective camber effects shifted the lift-curve upward and caused a considerable increase in $C_{l,\max}$ and a substantially intensified peak nose-down C_m and $C_{w,\text{cw}}$; the dynamic-stall angle α_{ds} at which the $C_{l,\max}$ occurred, however, remained unchanged (Table 1). Also, similar to the upward TEF motion, the phase angles at which the transient LEV effects occurred were not affected. The later the downward actuation, the smaller the net torsional damping (Table 1). No noticeable variation in C_p, regardless of t_s and $\delta_{\max}$, was observed during the post-stall flow process (Fig. 5d).

IV. Conclusions

The effects of prescheduled TEF motion on the dynamic-load loops of an oscillating NACA 0015 wing were investigated. For attached-flow oscillations, as expected, the values of $|-C_{m,\text{peak}}|$ and $C_{l,\max}$ were decreased for upward flap deflection and were higher with earlier flap actuation. Opposite trends were observed for downward flap deflection. Moreover, depending on the magnitudes of t_s and $\delta_{\max}$, the unsteady boundary-layer flow could become

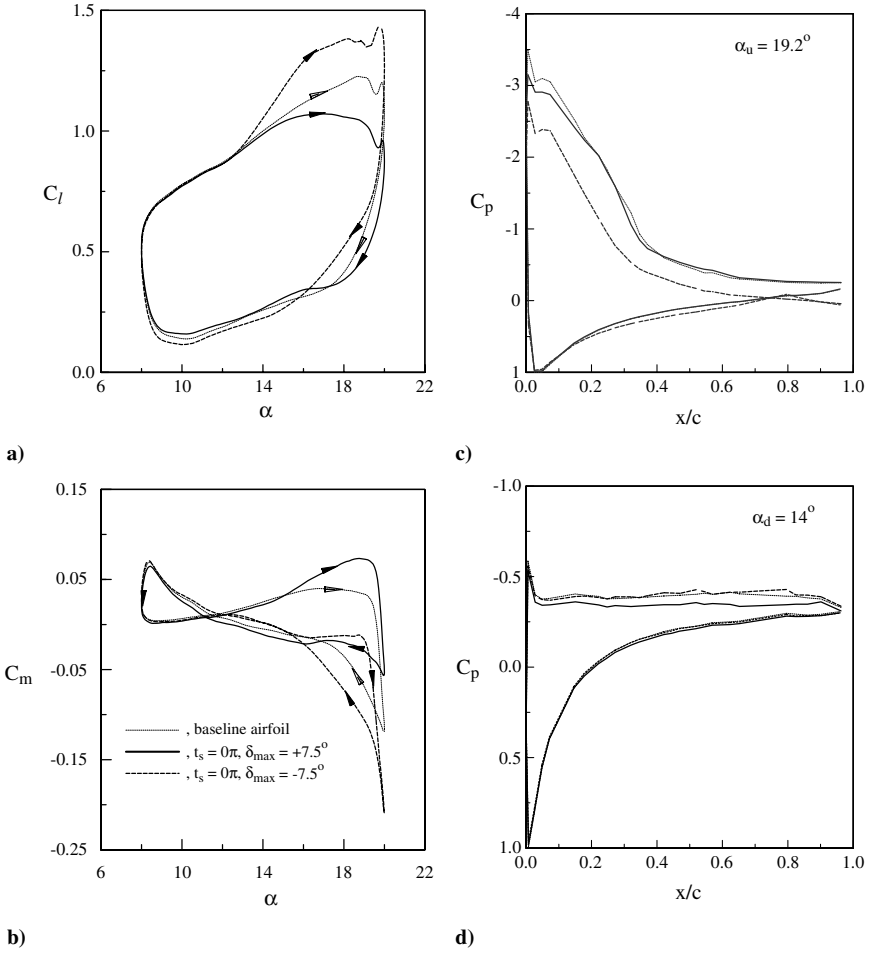

Fig. 5 Effect of TEF motion on C_l, C_m, and C_p for $\alpha(t) = 14\,\mathrm{deg} + 6\,\mathrm{deg}\,\sin\omega t$.

detached and a brief light-stall oscillation flow was introduced into the otherwise baseline-wing attached flow. For upward TEF control, no LEV formation was promoted, whereas a large C_l hysteresis, as a result of flow separation induced by the flap during pitch-down, and substantially increased positive C_w values were observed. For light-stall oscillations, no noticeable change in the phase angle at which the initiation and detachment of a LEV, independent of the values of t_s and $\delta_{\max}$, similar to deep-stall oscillations, was observed. The earlier the downward actuation, the larger the change in the net torsional damping was observed.

References

[1] Rennie, R., and Jumper, E. J., "Experimental Measurements of Dynamic Control Surface Effectiveness," *Journal of Aircraft*, Vol. 33, No. 5, 1996, pp. 880–887.

[2] Vipperman, J. S., Clark, R. L., Conner, M., and Dowell, E. H., "Experimental Active Control of a Typical Section Using a Trailing-Edge Flap," *Journal of Aircraft*, Vol. 35, No. 2, 1998, pp. 224–229.

[3] Enenkl, B., Kloppel, V., Preibler, D., and Janker, P., "Full Scale Rotor with Piezoelectric Actuated Blade Flaps," *28th European Rotorcraft Forum*, Royal Aeronautical Society, London, 2002.

[4] Feszty, D., Gillies, E. A., and Vezza, M., "Alleviation of Airfoil Dynamic Stall Moments via Trailing-Edge-Flap Flow Control," *AIAA Journal*, Vol. 42, No. 1, 2004, pp. 17–25.

[5] Gerontakos, P., and Lee, T., "Dynamic Stall Flow Control via a Trailing-Edge Flap," *AIAA Journal*, Vol. 44, No. 3, 2006, pp. 469–480.

[6] Lee, T., and Gerontakos, P., "Investigation of Flow over an Oscillating Airfoil," *Journal of Fluid Mechanics*, Vol. 512, 2004, pp. 313–341.

[7] Leishamn, J. G., *Principles of Helicopter Aerodynamics*, Cambridge Univ. Press, New York, 2002, pp. 379–389.